4-27-2017

Magnetic Position Sensor: Modeling a DC Electric Motor's Magnetic Interference

Aleksander Gust
College of Saint Benedict/Saint John's University, AFGUST@CSBSJU.EDU

Magnetic Position Sensor: Modeling a DC Electric Motor's Magnetic Interference

Aleksander Franklin Gust

St. John's University

Abstract

Measuring where an object is located is an invaluable tool across many disciplines. An emerging technology utilizes the magnetic field readings of a known source to locate where the object is in space. This type of sensor is useful since the target object can be measuring without contact, such as measuring the position of a piston through a cylinder wall. However, many problems arise since magnetic fields combine and distort when multiple fields are present. The magnetic disturbance has not been characterized for magnetic sensors in close proximity to DC electric motors. By modeling the known magnetic field source and gathering data of the distorted signal, a model of the DC motor field can be developed and later filtered out of the raw signal. In this thesis, a model for the magnetic field of a dipole magnet combined with that of a DC motor is explored in order to filter out the magnetic disturbances and regain the dipole field necessary for accurate position measurements. A characteristic DC magnetic field offset along with oscillations of the measured field has been shown to be attributed to the DC electric motor's influence and has been modeled.

Magnetic Position Sensor: Modeling a DC Electric Motor's Magnetic Interference

Introduction

The ability to distinguish an object's spatial location is an invaluable tool in many distinct fields of research. This is often done by measuring a certain physical trait of the target object that varies by its spatial location relative to the measurement device. Measurements are often converted to electrical signals which can be easily transferred and manipulated by a signal processing unit. Measurement devices that output electrical signals as a function of position are called position sensors. Often these position sensors require contact with the target object in order to measure its movement. However, coming into contact with the object you are measuring will change its state, and will continuously change the way it moves if the contact is continuous. In answer to this dilemma, non-contact position sensors have been designed to measure spatial location by not touching the target object. Often times these sensors require line of sight with the target object as they strike the object with pressure or electromagnetic waves and measure how the resultant wave changes as it returns to the sensor. However, instances arise when neither contact nor line of sight of the target object are available to the position sensor.

Position sensing without contact or line of sight requires the measurement of an intrinsic physical property that is distinguishable with position. One such physical property is the magnetic field given off by the target object. Permanent magnets will project a consistent magnetic field that is differentiable with respect to the magnet's position relative to a measuring device. This relationship allows for complete spatial resolution of the target object as long as a clear, distinct magnetic field can be measured. This opens up numerous possibilities of measuring the target object's position through obstacles, such as the position of a piston through an enclosed cylinder casing. Perfecting a sensor such as this could lead to many non-invasive alternatives for measuring the physical positions of magnetized objects.

The University of Minnesota's Dr. Saber Taghvaeeyan and student Ryan Madson have been developing such a sensor the past few years. Utilizing neodymium dipole magnets as target objects, they have developed a working prototype of the sensor. The sensor uses Anti-Magneto Resistive (AMR)

magnetic field sensing microchips paired with the theoretical knowledge of the magnetic field produced by a dipole magnet to accurately determine the position of the magnet. The sensor has an onboard microcontroller to gather the raw magnetic field data, filter the data, and transform the readings to a usable analog voltage output varying linearly with the linear position of the magnet. This prototype has been proven to work through relatively thick metal hydraulic cylinder walls with only a small dipole magnet attached to the piston head inside the cylinder. However, the accuracy of the sensor depended on the consistency of the magnetic field reading.

Complications arose when random ferrous objects passed near the sensors. This would cause the magnetic field to exhibit strange behavior which would not be normal for the average dipole field, this in turn caused abnormalities in the position measurement. Therefore, the UMN team utilized a predictive filter which would remove abrupt changes in the magnetic field that would be caused by such a disturbance. While these abrupt disturbances could be easily filtered out, expansive external disturbances could not.

The external magnetic fields measured in a laboratory setting, such as the Earth's magnetic field, appear very constant compared to the field of the moving magnetic dipole. Because of this, the external fields can be easily filtered out, allowing for solely the dipole field to be acquired. This is not true for electronic components with high current draw in close proximity to the sensors. An electric DC motor draws current through a rotating armature between a permanent magnet. This produces torque on the armature shaft causing it to rotate (Horowitz and Hill, 2015). This rotating loop of current creates a distinguishable magnetic field that is picked up by the magnetic sensors. Due to the superposition principle of electromagnetic field interactions, the dipole field of the magnet and the DC motor's external field are summed together at the magnetic sensor location creating a distorted and nearly unusable magnetic field signal for target position identification purposes (Griffiths, 2013). The focus of this research is to characterize the disturbance contributed by the DC electric motor as the Electro-Hydraulic Actuator is driven. A model of this disturbance is explored in order to better understand the distorted

signal output from the magnetic sensors. The model of the DC motor's magnetic field is then used to filter the output signal to regain the original dipole magnetic field.

Methods and Materials

The experimental setup necessary to conduct this research consisted of an electrohydraulic actuator, a sonar displacement sensor, 3 magnetic field sensors, two power supplies, and a microcontroller.

Experimental Apparatus

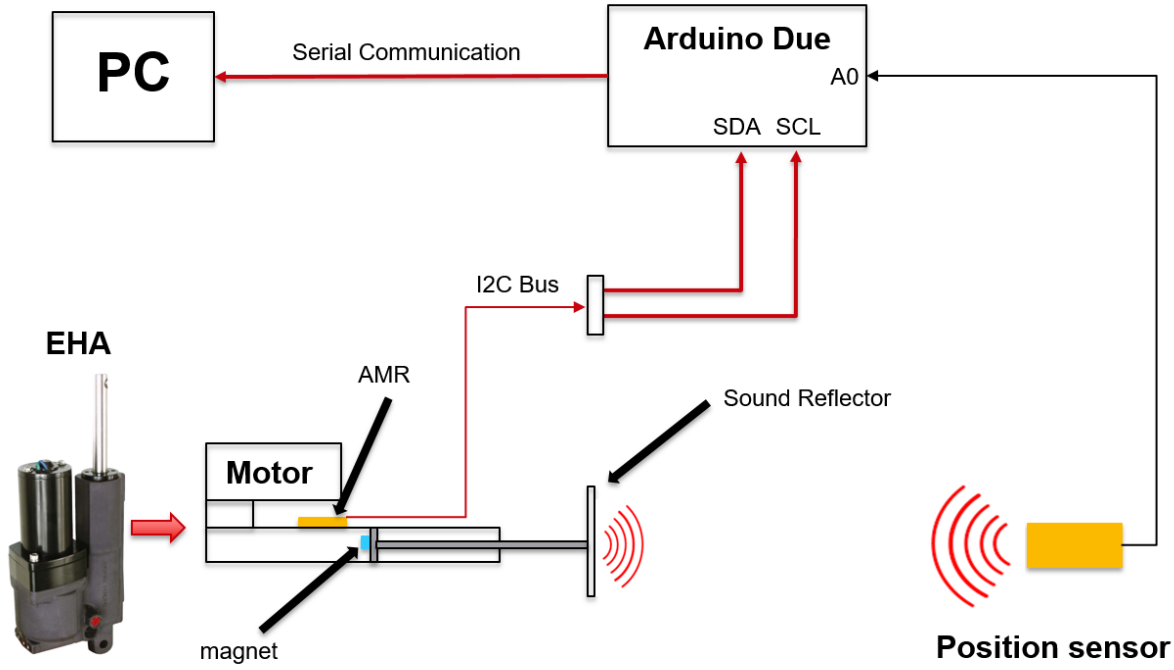

Figure 1. Diagram of apparatus used for experimentation. The yellow blocks indicate sensors, the red signal wires indicate serial communication, the black wire indicates an analog signal. Neither of the two power sources driving the EHA or position sensor are shown.

A Parker Compact Electro-Hydraulic Actuator (EHA) was used as the primary mover. This actuator operates by using a DC electric motor to turn a hydraulic pump. This hydraulic flow is then directed through a check valve and into the cylinder which in turn drives the piston

outward. To retract the piston, the current supplied to the DC motor is reversed, driving the pump in the opposite direction and forcing hydraulic fluid into the other side of the cylinder causing the piston to retract (Parker, 2011). The U-GAGE T30UX ultrasonic position sensor utilizes sound waves that are emitted at a known energy level. The sound waves then bounce off the target and return to the sensor at a lower energy level. Distance measurements are obtained through physical relations between the speed of sound through air (as a function of ambient temperature) and the time difference between the emitted sound wave and the resultant reflected sound wave (Banner, 2015). Three, 3-axis Honeywell Anti-Magneto Resistive (AMR) sensors were used to detect the magnetic field signatures of the moving EHA piston with attached magnet (see Figure 2).

Magnetic Sensor Breakout Board

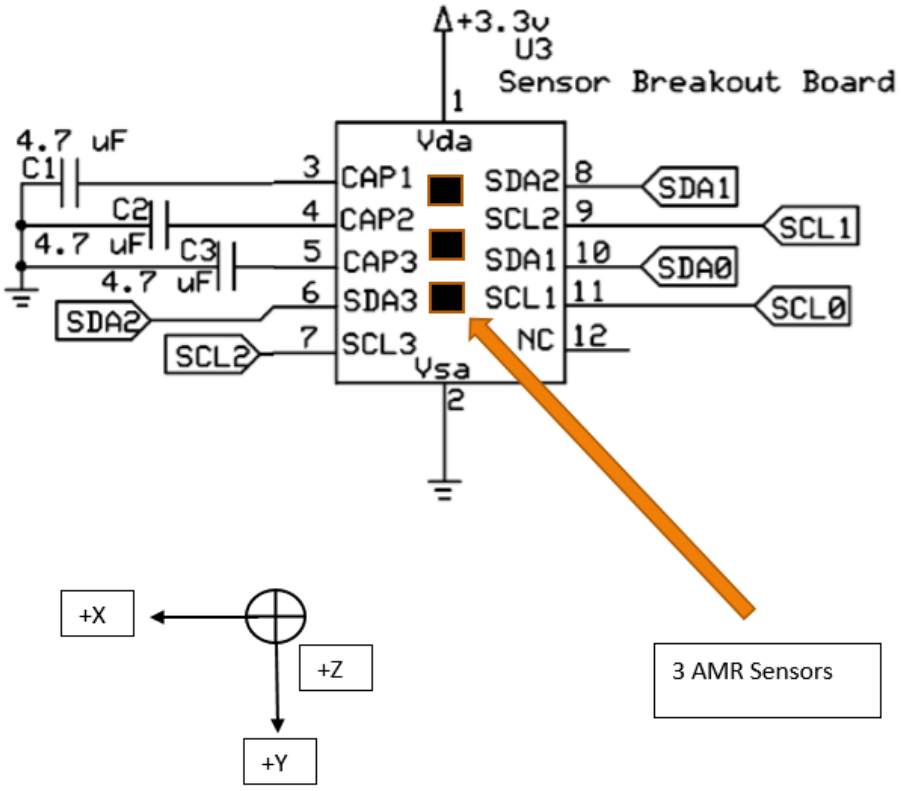

Figure 2. PCB breakout board with pin configurations for I2C communication protocol for serial transmission of data from the AMR sensors. The orientation of the sensors is not traditional, being that the z-coordinate goes into the page. PCB is mounted on EHA to align with the actuator along the y-axis.

AMR material changes its resistive properties when subjected to a magnetic field. Utilizing this material in a Wheatstone Bridge configuration allows for a direct correlation between the AMR material's resistive value and a resulting output voltage (Horowitz and Hill, 2015). Arranging three AMR Wheatstone Bridge configurations to form an orthogonal set of axes allows for the complete magnetic field reading at a point in Euclidean space (Taghvaeeyan, 2014). Two power supplies were used: a Mastech HY7530EX DC Power Supply, and a Lambda Regulated Power Supply Model LL-902-OV. The Mastech was used to drive the EHA's DC

motor and the Lambda was used to power the U-GAGE ultrasonic sensor. The microcontroller used for data collection was an Arduino Due.

The AMR sensors were placed on a PCB board allowing for pins to be soldered on for use with a breadboard (fabricated by UMN team). This PCB board contained all three AMR sensors, each with output pins for I2C communication with the Arduino. Each AMR chip had the same address, therefore wiring all three to a single SDA and SCL bus would not follow I2C protocol. An Adafruit TCA9548A Multiplexer was used to multiplex the SDA and SCL lines of each AMR sensor into one long serial message identified by the new multiplexer address. The new SDA and SCL lines were fed into the Arduino Due's respective input pins and connected via micro USB to the desktop computer. Analog voltage input for sonar reference displacement sensor also needed to be communicated to the Arduino. The Arduino's analog voltage input pin is rated for 0-3.3V max; however, the U-GAGE sensor was configured to have an output voltage reading of 0-10V with respect to 10-100cm of separation from the sensor and its target. Therefore, a voltage divider was implemented to reduce the voltage output of the sonar sensor to 0-3.3V in order to protect the Arduino. The output of this voltage divider was placed into the A0 analog input pin on the Arduino and the ground wire for the sonar sensor was placed into the Arduino GND pin to provide a reference for the analog input.

MATLAB was then configured to open a serial port and read in the now combined SDA and SCL signals with an agreed upon baud rate of 115200 bits per second. Since MATLAB only viewed this signal as a serial list of values, it was necessary to separate each complete message by performing a loop that counted the number of bytes that would make up a total message. The complete single message would then be deconstructed further to fill an array consisting of each AMR sensor's 3-axes of magnetic field readings (9 signals total), the sonar reference

displacement sensor analog output, and the clocking associated with the readings to provide a consistent data set. Once the raw data had been acquired and separated in MATLAB, further analysis could be completed.

To gather the experimental data, a controlled set of tests were executed. The test rig consisted of the EHA secured at one end of the work bench and was driven by the high wattage Mastech power supply. Facing the EHA 35cm away was the U-GAGE sensor which was aimed at a secured cardboard target attached to the piston of the EHA. For protection from stray sound and for ease of mounting the U-GAGE sensor, a protective cardboard box had two holes cut on either side, one to mount the sensor and the other to allow the piston to move back and forth within the box. The sonar sensor was powered by the Lambda power source and the output of the sensor was fed into the voltage divider on a separate breadboard. The AMR sensor PCB board was placed on a small breadboard which contained adhesive on the opposite side. After making the proper connections from the PCB to the Arduino, this small breadboard was adhered to the EHA directly underneath the DC motor and above the linear travel of the piston. This configuration placed the 3 AMR sensors in succession on the axis of travel of the EHA piston while the adhesive assured consistent placement during tests.

The first test was to gather a baseline reading of the magnetic field of the dipole magnet connected to the EHA piston head as a function of displacement. To do this, the piston was completely retracted to begin testing. Then the Mastech power supply was set to +15V to power the EHA and the Lambda power source was set to +13V to power the sonar sensor. The MATLAB program to gather data was executed and the data was saved in a file. After this was complete, the Mastech sourced 10A of current to the EHA DC motor extending the piston about 1cm. After sufficient time for the magnetic field from the DC motor to have dissipated, the data

collection was initiated again. This continued until the length of the piston had been mapped. This data was placed within a look up table within Simulink to be used in the simulation of the magnetic field. This was the baseline expected field, if any variation of this field showed up while gathering data with the DC motor running we could attribute this disturbance to the DC motor.

The next test was to determine how the magnetic field of the DC motor affected the dipole magnetic field. This test consisted of retracting the piston to the starting point, and then initializing data collection for a time of 30 seconds. During this 30 seconds, 10A of current was sourced from the Mastech to the EHA to extend the piston completely while data was being gathered (see Figure 3).

Magnetic Field Readings of Dipole Magnet

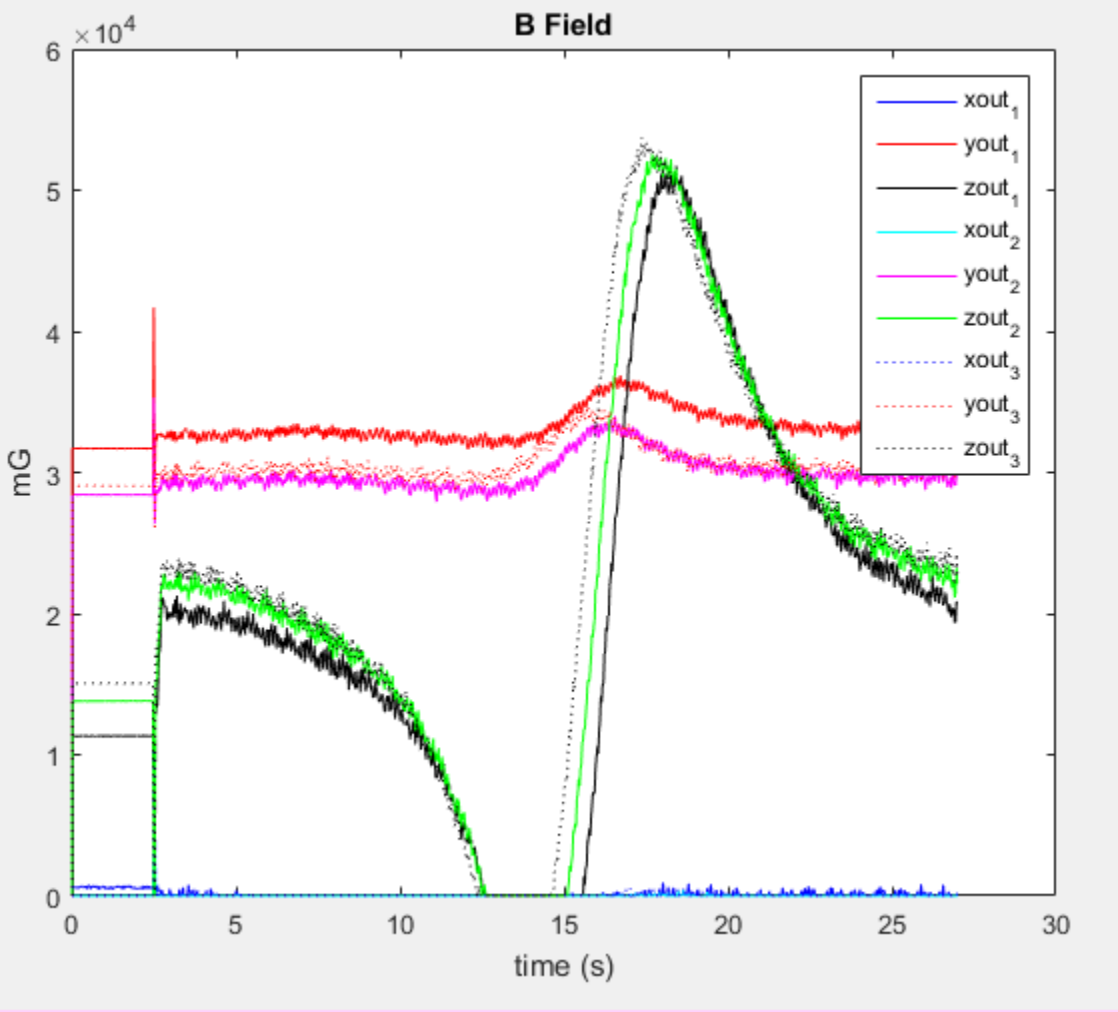

Figure 3. Magnetic field data of dipole magnet attached to extending piston of electro-hydraulic actuator. Magnet passes underneath 3, 3-axis Honeywell Anti-Magneto Resistive (AMR) sensors each separated by one millimeter on PCB board, resulting in 9 distinct magnetic field signals. The large disturbance at the beginning and end of the 20 second duration test indicates the 12V DC motor initializing/terminating 10A current draw.

This data resulted in a similar wave form as the look up table, however there was a noticeable DC offset along with an oscillating disturbance. The gathered signal was converted into a magnetic field vs displacement look up table in Simulink and a simulation was ran to determine the differences between the baseline field and the tested field.

Data and Results

The experimental data used for this analysis was gathered utilizing the previously described process and is depicted by Figure 3 above. Figure 3 contains all nine magnetic field readings from the three AMR sensors. The signals of interest are that of the y-axis component of the dipole field and the displacement signal (see Figure 4).

Magnetic Field of Moving Piston

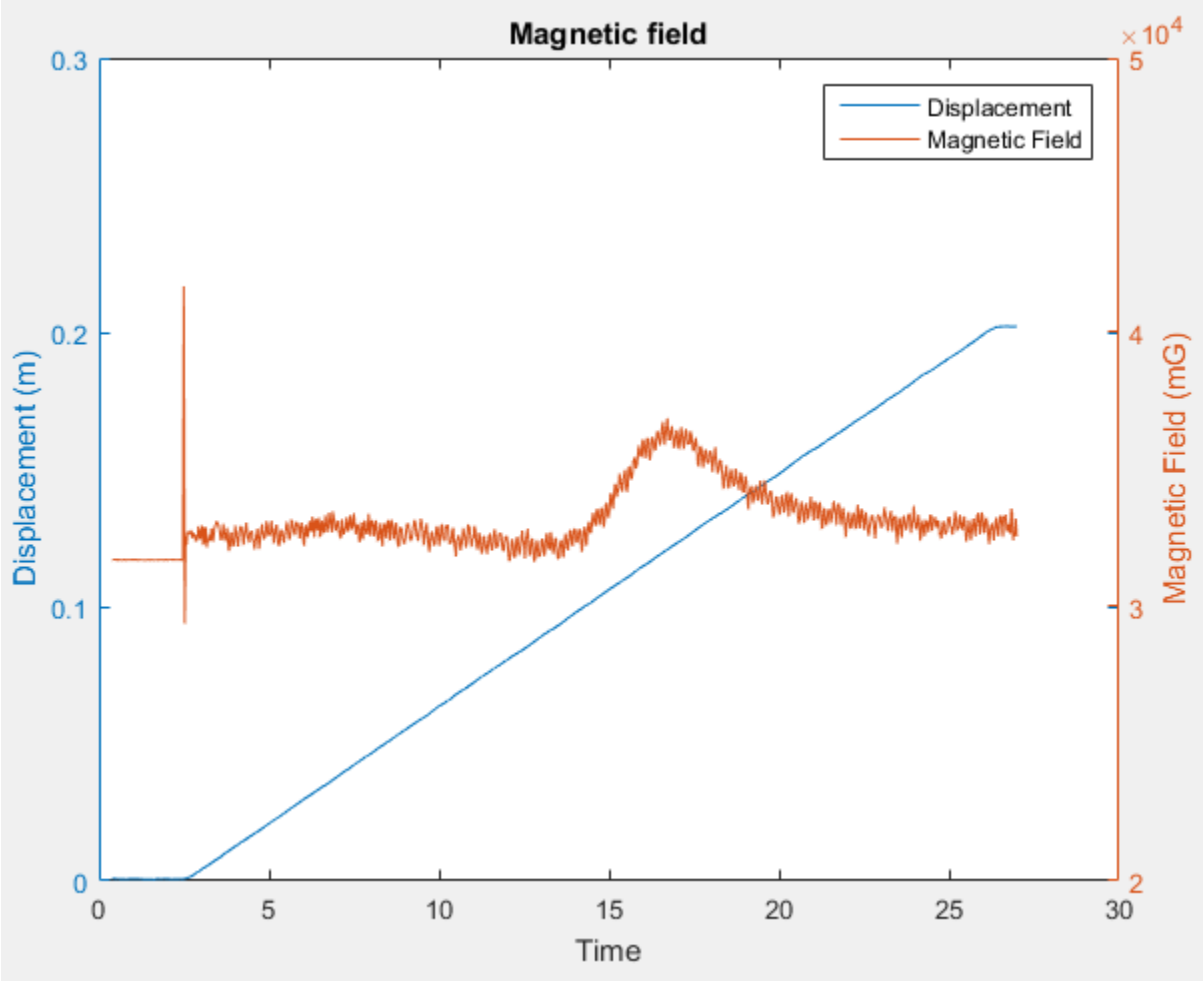

Figure 4. Magnetic field data of dipole magnet attached to extending piston of electro-hydraulic actuator compared to the displacement of the piston. The large disturbance at the beginning and end of the 20 second duration test indicates the 12V DC motor initializing/terminating 10A current draw.

A moving average filter was deemed necessary in order to reduce data size and smooth the signal for use in simulation (see Figure 5).

Filtered Magnetic Field Signal

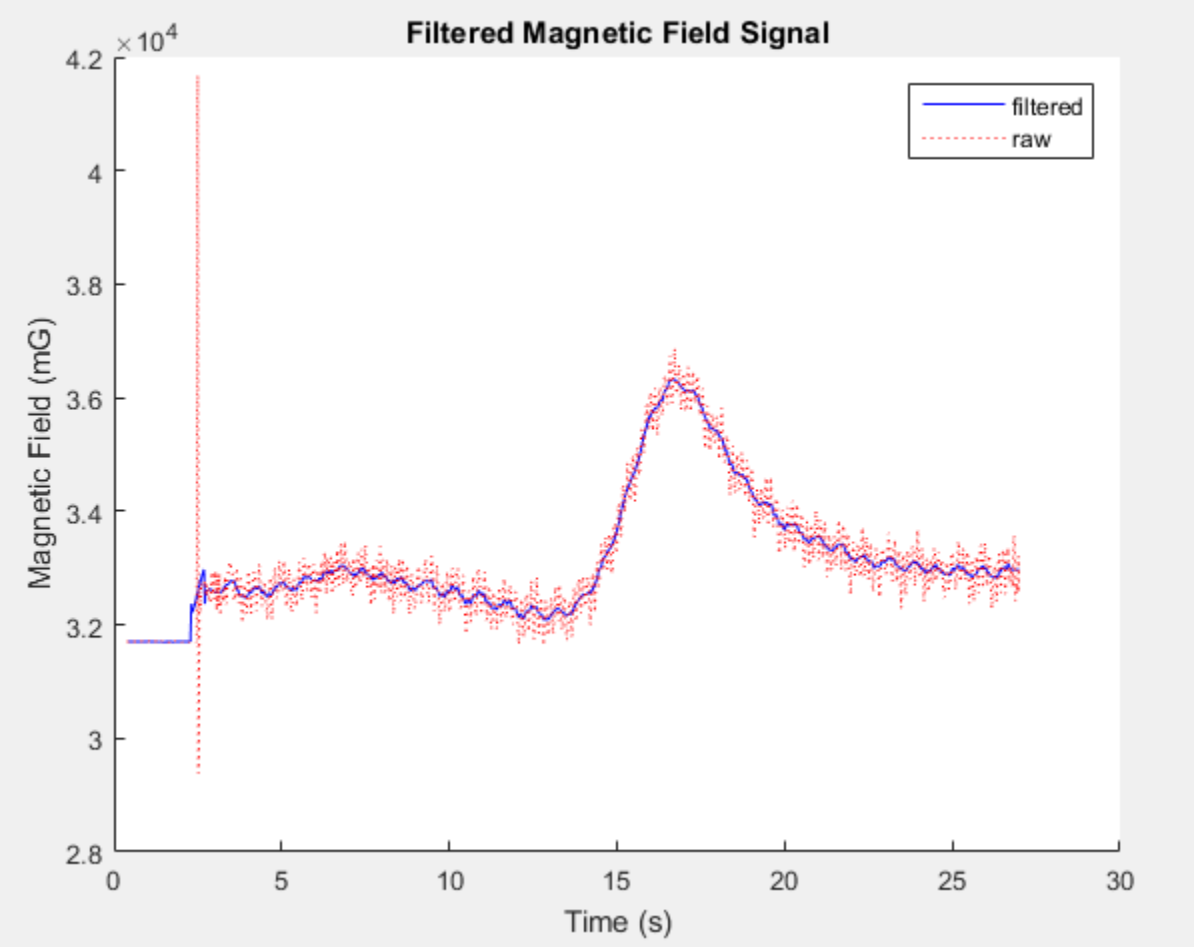

Figure 5. Raw magnetic field data before and after a moving average filter has been applied.

By averaging the first initial data points before the EHA was energized, the constant magnetic field of magnitude 3.15e4 mG gathered by the AMR sensors was subtracted from the signal. This left only the field created by the dipole magnet and the DC motor. It became apparent that there was an irregular DC offset along with oscillations combined with the dipole

field. The modeled magnetic field of the dipole is shown in Figure 6, and further illustrates the abnormality of the measured noise in comparison to the sole dipole field.

Modeled Magnetic Field of Moving Piston

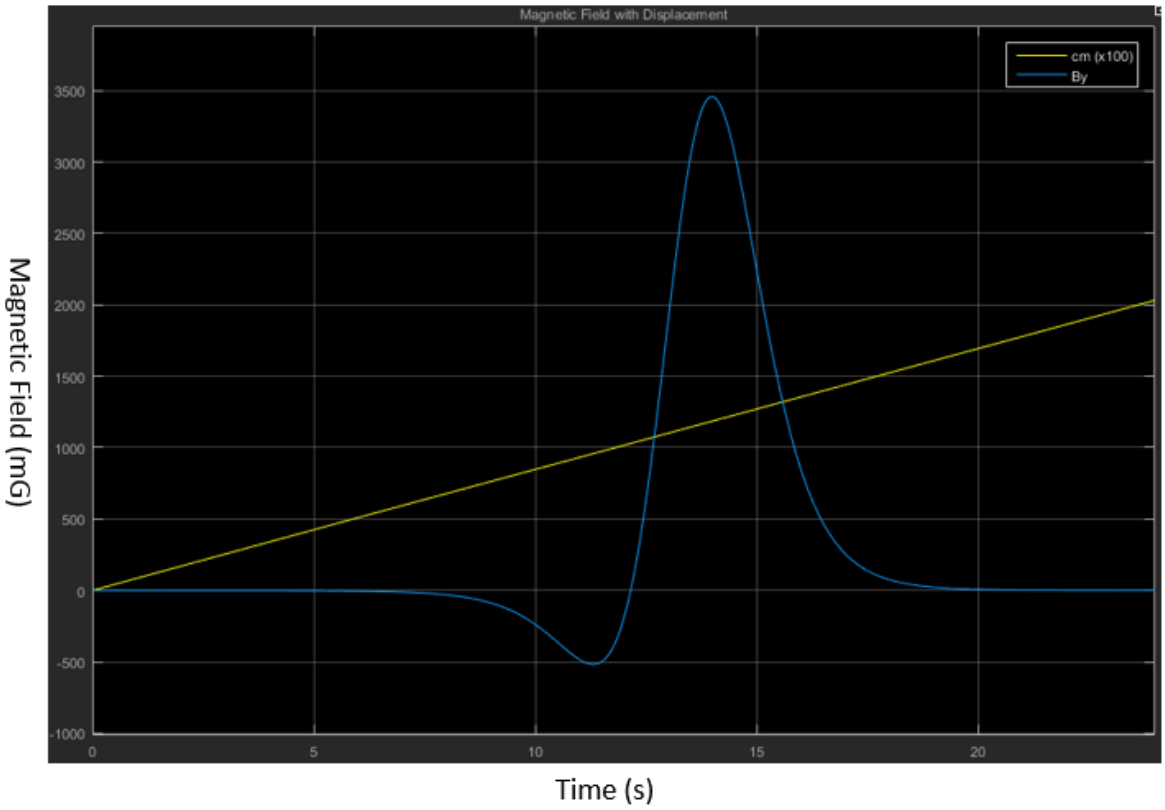

Figure 6. Modeled magnetic field data of dipole magnet attached to extending piston of electro-hydraulic actuator compared to the displacement of the piston. This was simulated using Simulink with a simulation run time of 24 seconds as consistent with experimental test times.

Next came the process of modeling the DC motor's magnetic field contribution. The DC offset of the magnetic field caused by the electric motor was experimentally determined to be about 1,121 mG. This was also obtained by averaging the subset of data gathered that did not contain traces of the dipole field. Along with this DC offset, a noticeable oscillation of the magnetic field caused by the electric motor was found. This oscillation was replicated using a sine wave of amplitude 220 mG and frequency $(8\pi)/3$ rad/sec. The oscillating contribution to the

magnetic field was assumed to originate from the rotational motion of the electric motor armature. By summing these two signals together, a model of the DC electric motor was created. Summing this signal with that of the modeled dipole, a more accurate model of the magnetic field captured by the AMR sensors was acquired and is shown in Figure 7.

Simulated vs. Experimental Field

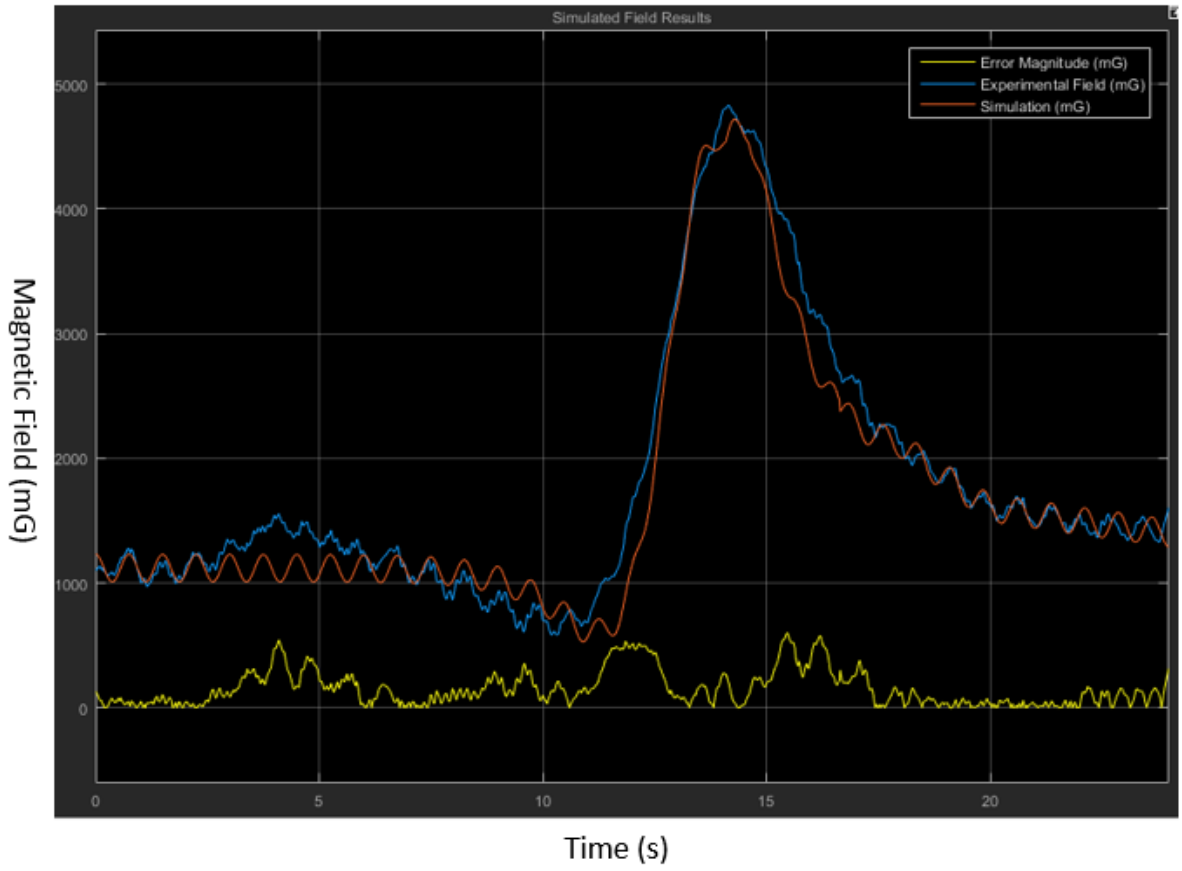

Figure 7. Simulated magnetic field compared with experimental data of magnetic field. This 24 second simulation contained modeled disturbances contributed by the DC electric motor superimposed on the baseline dipole magnet field.

With a reasonable working model of the DC electric motor, an attempt at filtering the raw data and then transforming the filtered magnetic dipole field back into position measurements was accomplished. The high-level overview of the Simulink model can be viewed in Figure 8.

Magnetic Field Simulation

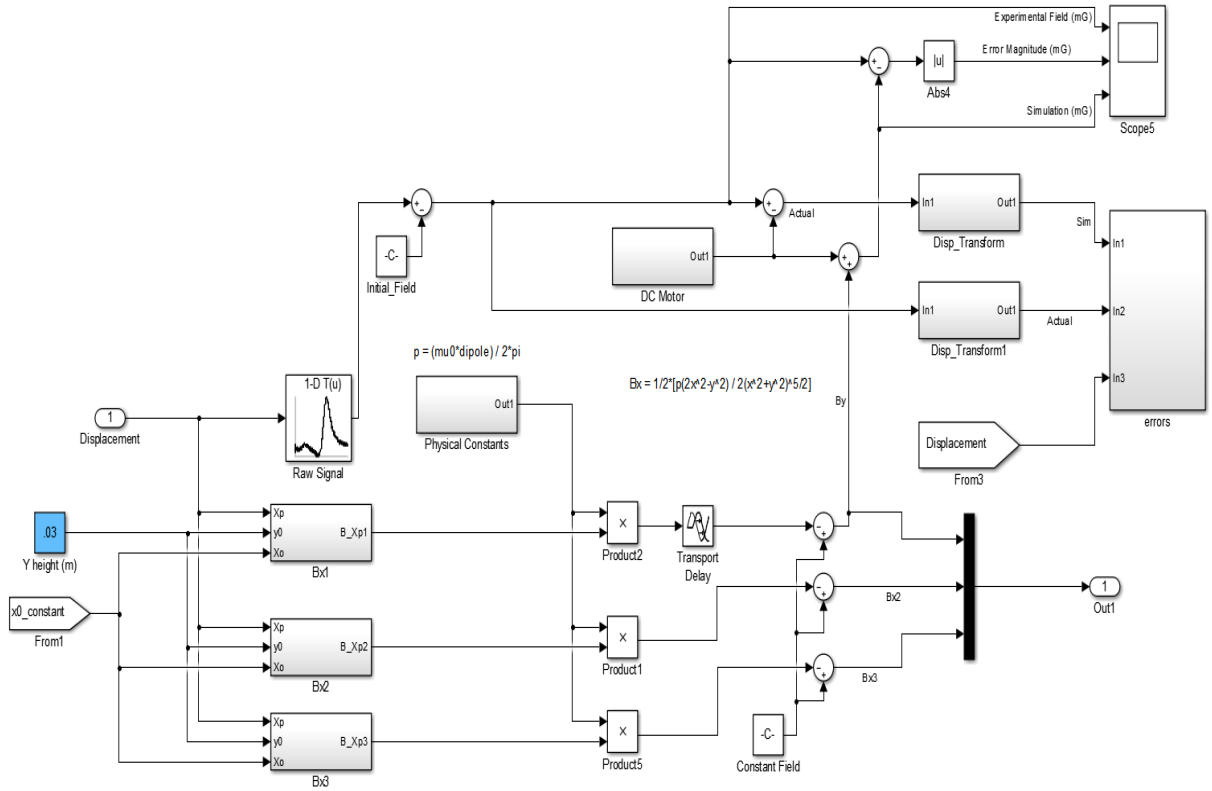

Figure 8. This figure shows the overall flow of the Simulink simulation of the magnetic positioning sensor. A user defined y-axis initial position (distance sensor is vertically away from the magnet position, in this case 3cm) was implemented as a variable input. The user can also configure their own cylinder position signal to test different ranges of motion. The displacement signal from the sonar position sensor was used in this experiment. Both of these signals are fed into the dipole magnet model to recreate the expected dipole field. Modeled DC electric motor magnetic noise is then simulated and added to the dipole field. The theoretical model of the field was used to tune the DC motor sub-block to recreate the experimental observations and was then used to filter the raw signal.

There are many sub-blocks integrated into this model, however the few of interest to the reader are the 1-Dimensional look-up table of the experimentally gathered raw data as a function of position, the dipole field model sub-block, the DC electric motor sub-block, and lastly the displacement transformation sub-block.

The raw data was compiled into a look-up table of magnetic field readings as a function of the dipole magnet position gathered by the sonar sensor. This was used to recreate the same signal wave-form regardless of the variable magnet displacement input to the simulation. The signal generated by the look-up table was then modified within the simulation and also used for analysis purposes. The DC motor sub-block contains the model of the electric motor described above and was used to modify the raw data signal. By subtracting the DC motor field from the raw signal, a signal resembling that of the modeled dipole magnet was produced. Both the raw data signal and the filtered signal were then fed into the displacement transformation sub-block to obtain the position of the magnet as a function of its magnetic field value.

Transforming the magnetic field signal into a displacement signal was then attempted. This was problematic in Simulink since the model of the dipole field was not an injective function. An injective function meaning every element of the domain is not strictly mapped to a single element in the codomain and could be mapped to multiple elements in the codomain. A position value could have the same magnetic field value at multiple points, and therefore is not invertible. In order to create a look-up table of displacement as a function of magnetic field, a new approach had to be considered. It was necessary to find the extrema of the dipole field strength and create subsets of the displacement range in a piece-wise fashion. The extrema points were determined by numerically calculating the derivative of the dipole field and locating the zeros. A set of three 1-dimensional look-up tables were then produced that would cover the entire range of motion of the magnet. At points of extrema, the active look-up table would switch to the next look-up table, allowing the entire path of the magnet to be mapped by the changing magnetic field. The displacement transformation sub-block can be viewed in Figure 9 below.

Displacement Transformation Sub-block

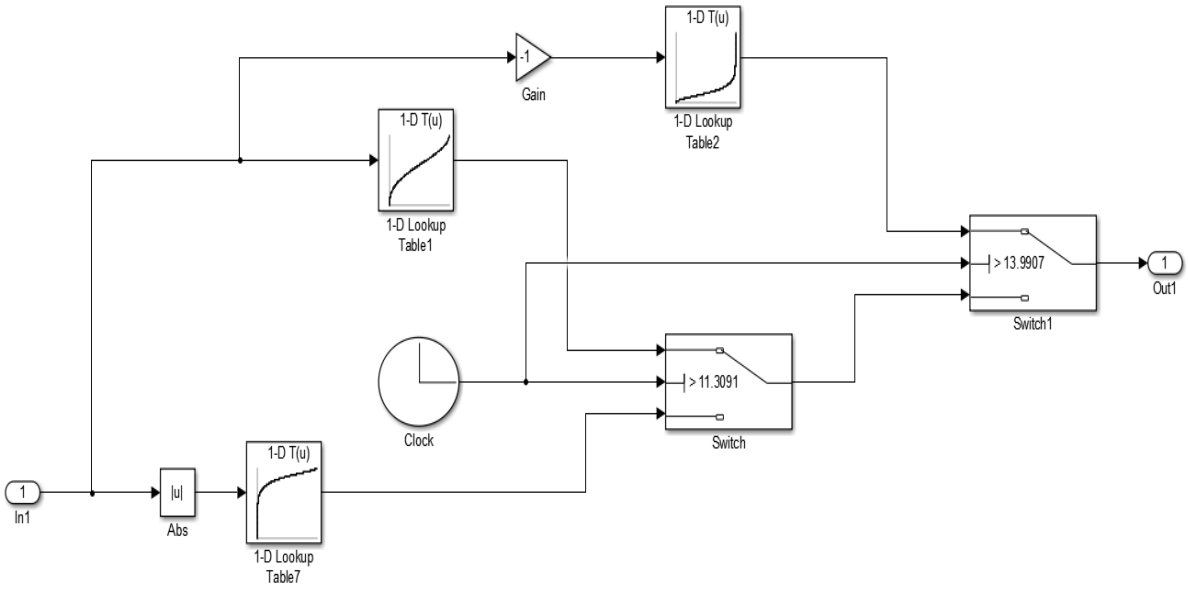

Figure 9. The displacement transformation sub-block contained the look-up tables necessary to convert theoretical dipole magnetic field strength into a relative position value. Three separate tables were necessary since the magnetic field strength of a dipole is equivalent at multiple positions and therefore was non-invertible without using this method in the simulation. The simulation clock was used as the switch triggering signal in this simulation for convenience; however, a numerical derivative of the magnetic field signal run through a zero-crossing detection block would also trigger the simulation correctly.

Results of the transformation were to be expected with such a noisy signal, for only a pure dipole field would accurately map the entire magnet's path. As depicted in Figure 10, the displacement transformation was only reasonably accurate within the range of large magnetic variation caused by the magnet.

Displacement Transformation

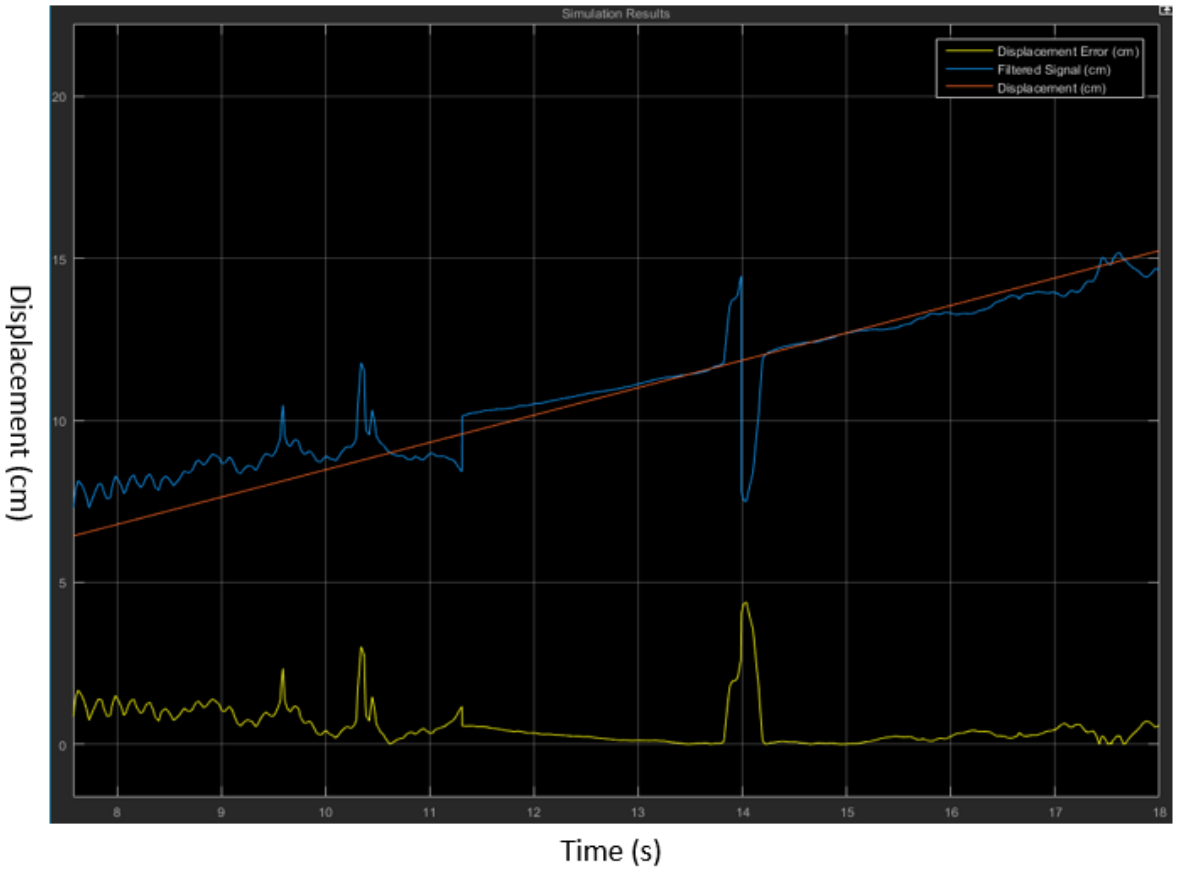

Figure 10. This is a subset of simulation data to better show the results of the position resolution. The magnetic field signal was not distinguishable near either end of the piston range of motion and therefore did not yield unique results from the displacement transformation. Reasonable position resolution was obtained during the 10-15 cm position range where the dipole field is most pronounced and easily distinguishable relative to the electric motor noise. The large irregularity at time 14 seconds was the peak of the dipole field spike and is due to a small difference in the filtered signal compared to the simulated signal, which constitutes a large error at such high magnetic field values.

Towards either end of the magnet position range, the magnetic field is not discernable enough to provide an accurate resolution of its position. However, between the highly variant field range a reasonable resolution of position was obtained to well within a centimeter. Unfortunately, there were some noticeable differences between the modeled magnetic signal and

the filtered raw signal near the dipole spike of the fields. Referring back to Figure 7, one can see a noticeable discrepancy at the peak of the of the dipole spike when comparing the modeled field to the experimental field. A large position error is attributed to this variance since a small inconsistency at the tail end of this look-up table subset, near the ending extrema point, constitutes for a large variation in position. However, the filtered signal still greatly outperforms the unfiltered displacement transformation shown in Figure 11.

Experimental vs. Filtered Displacement Transformation

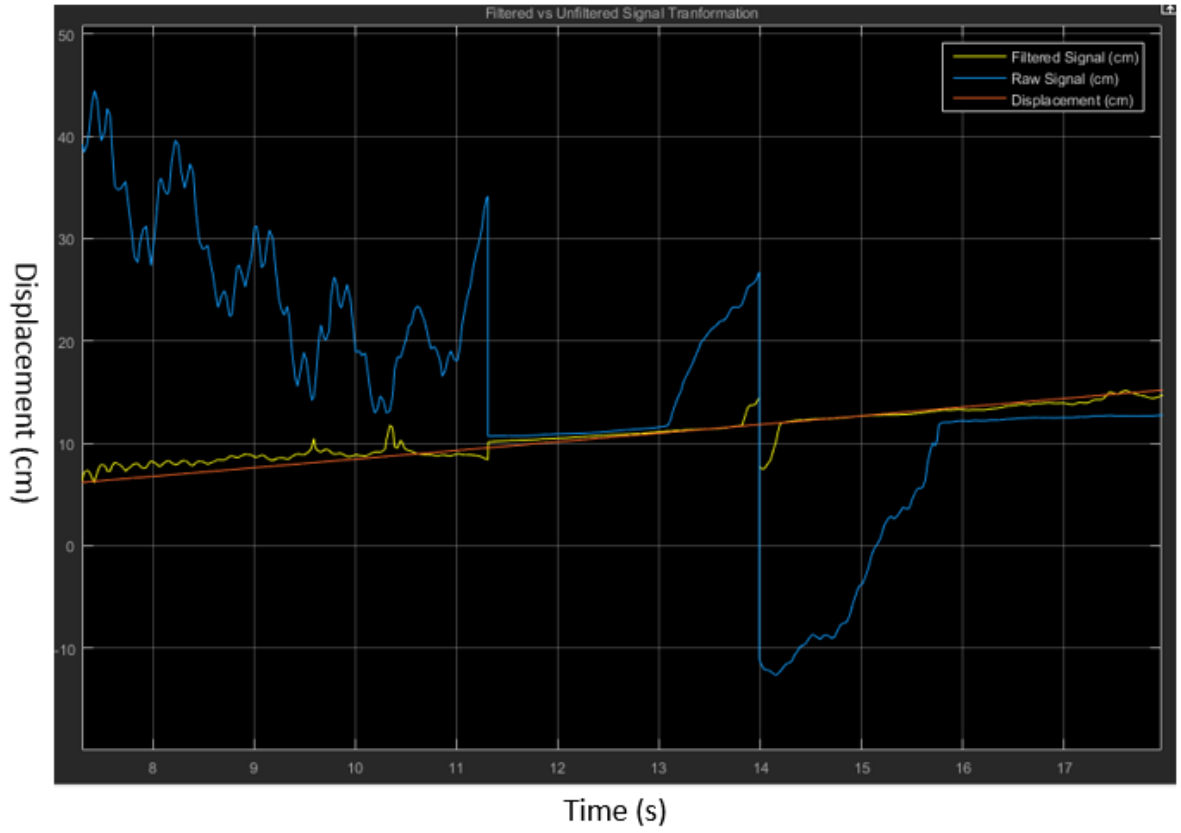

Figure 11. The simulation results for the same time frame as Figure 9 using both the raw and filtered signal in the displacement transformation simulation. This figure depicts the large discrepancies between position resolution when comparing the two signals. Most notable are the dipole spike irregularity and the oscillating signal in the 8-11 second range. The large error near the dipole spike was caused by the electric motors dc offset which resulted in a larger difference between the modeled field and the measured field. The oscillating signal was caused by the electric motor's magnetic field oscillations which then transferred to an error in position resolution.

This figure also helps show how the dipole field strength becomes more pronounced as it travels underneath the AMR sensors and therefore converges reasonably well onto the magnet position during those sections for both raw and filtered signals.

Conclusion

The research conducted has shown a noticeable effect on the magnetic field readings of AMR sensors attempting to sense the dipole magnetic field of a target magnet when in close proximity to an electric motor. The novel disturbance was explored for this application and a simple model for its effects was developed. A previously unusable raw signal gathered by the AMR sensors was filtered to reasonably resemble the sought-after dipole magnetic field. A simulation of the entire system was developed and used to visualize, filter, and invert the magnetic field data back into the relative position of the target magnet attached to the piston head of the EHA. Error in the position calculation is, admittedly, substantial considering the distances mapped. However, the position error attributed to the unfiltered signal is of a much greater magnitude and often corresponded to impossible position measurements when considering the distances mapped.

Determining the position of an object with the restrictions of not having line of sight, direct contact, or reconstructing a system in an invasive way is quite important in many fields of research, engineering, and sensing technologies. Determining new and effective filtering techniques for magnetic field data is paramount to the functionality of this type of sensing technology. Filtering raw magnetic field data is difficult in the respect that many different sources can combine in magnitude rendering the data gathered useless, especially when disturbances are dynamic in nature.

The model of the DC electric motor proposed is quite basic and not all encompassing in regards to different loads placed upon the motor. Future research is needed to determine the effects of loading the actuator in order to stimulate increased current draw by the electric motor. This increased current draw will provide the motor with enough torque to turn the hydraulic

pump to push the load. I hypothesize that the increased current draw will also change the frequency of the rotation oscillation shown in the magnetic field as well as the magnitude of the dc offset of the magnetic field produced by the electric motor. Conducting this research will greatly benefit the development of an analytical model of the electric motor as a function of load/current draw. A more exact model of the electric motor will correspond to an increase in accuracy of the signal filter, which will aide in accurate resolution of the target magnet's relative position.

Inverting the magnetic field into the relative position of the piston proved to be difficult when using MATLAB and Simulink. This difficulty arose from the analytical definition of a dipole field being a surjective function. Surjective functions have elements in their codomain that are mapped to by multiple elements in their domain, meaning that the magnetic field value picked up by the AMR sensors would read the same value at different positions. Functions of this type are not directly invertible and need to be broken down into subsets that allow for one-to-one mapping of magnetic field value for a specific range of position values. The method described above to switch between these maps was flawed, and contributed to abrupt error fluctuation at the time the dipole spike was registered. An improved method could utilize the z-component of the magnetic field that registers the field perpendicular to the axis of piston motion. This field changes polarity at the time of the dipole spike and could be used to replace the derivative calculation of the y-component of the magnetic field previously used. Triggering the mapping subsets in this fashion would provide a smoother, real time transition since the spatial derivative need not be calculated. However, a filtering solution for this method must also be explored to prevent switching chatter if the field jumps between positive and negative values quickly while the magnet is passing underneath the AMR sensors.

References

Taghvaeeyan Saber. 2014. Exploiting Inherent Magnetic Signatures of Ferromagnetic Objects for Detection, Identification, and Position Estimation Applications. University of Minnesota.

Griffiths J. David. 2013. Introduction to Electrodynamics. Fourth Edition. Reed College.

Horowitz Paul, Hill Winfield. 2015. The Art of Electronics. Third Edition. Harvard University.

Parker. 2011. Parker Compact Electro-Hydraulic Actuator (EHA) Instruction Manual. Online. Retrieved from: https://www.parker.com/literature/Cylinder%20Europe/EHA%20Instruction%20Manual%203-11.pdf.

Banner. 2015. U-GAGE T30UX Series with Analog Output Specification Sheet. Online. Retrieved from: http://www.clrwtr.com/PDF/Banner/Banner-U-GAGE-T30UX-Series-Sensors.pdf.

Mastech. 2009. DC Power Supply HY3000-HY5000 Users Manual. Online. Retrieved from: http://hades.mech.northwestern.edu/images/f/f7/Mastech_power_supply_manual.pdf.